國立交通大學

光電工程研究所碩士班

碩 士 論 文

利用奈米金粒子增強螢光元件之研究

Surface Plasmon Mediated Fluorescence Enhancement
of Gold Nanoantenna

研 究 生：林宗瑋

指導教授：田仲豪　副教授

中 華 民 國 九 十 八 年 七 月

利用奈米金粒子增強螢光元件之研究

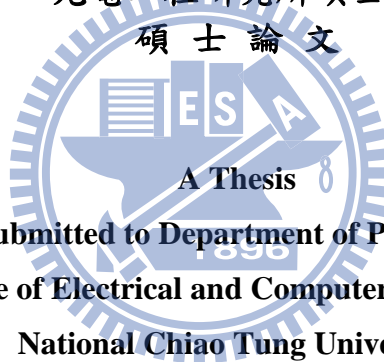# Surface Plasmon Mediated Fluorescence Enhancement of Gold Nanoantenna

研 究 生：林宗瑋　　　　　Student：Zong-Wei Lin

指導教授：田仲豪　　　　　Advisor：Chung-Hao Tien

國 立 交 通 大 學

光電工程研究所碩士班

碩 士 論 文

A Thesis

Submitted to Department of Photonics

College of Electrical and Computer Engineering

National Chiao Tung University

in partial Fulfillment of the Requirements

for the Degree of

Master

in

Department of Photonics

July 2009

Hsinchu, Taiwan, Republic of China

中華民國九十八年七月

利用奈米金奈米增強螢光元件之研究

學生：林宗瑋　　　　　　　　　　　　指導教授：田仲豪

國立交通大學光電工程學系碩士班

摘　　　要

藉由入射光與金屬奈米粒子的耦合,使得金屬表面周遭產生的強大的侷域性電場，此光學特性即稱為侷域性的表面電漿共振(LSPR)，目前已經廣泛被運用在生醫檢測、光電元件等多方面上。根據準靜粒子下的米氏理論(Mie Theory)，單一金屬粒子的光場表現如同一個奈米天線發出的場型，而我們研究在於一個層狀的高分子結構中，參雜在高分子聚合物(PEDOT:PSS)中的金奈米粒子(天線)與發光高分子聚合材料中(MEH:PPV)的激子之間耦合的關係。實驗中相對於未參雜的金奈米粒子的樣本中，我們得到了 2.3 倍的螢光量子增益。

有研究顯示：當發光體靠近金屬表面時會增強其激發效益，然而，過於接近會導致非輻射性的能量轉換到金屬粒子上，導致發光體的量子增益下降；在實驗中，藉由調整間隙層的厚度進而改變金屬奈米天線和發光層之間的距離，可得到一理想化的相對量子螢光增益。最後將此樣品的結構運用在電制發光的高分子聚合物系統上，在同樣的電性條件下，發光的量子增益能有效提升。
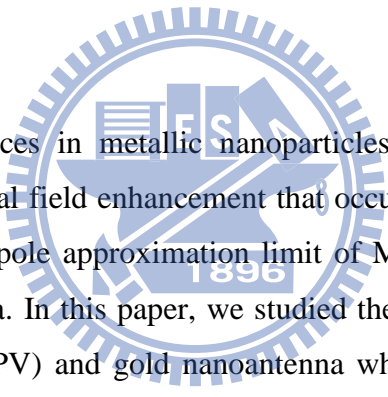
Surface Plasmon Mediated Fluorescence Enhancement
of Gold Nanoantenna

Student：Zong-Wei Lin　　　　　　　**Advisors：Dr. Chung-Hao Tien**

Department of Photonics
National Chiao Tung University

ABSTRACT

Surface plasmon resonances in metallic nanoparticles are of interest for a variety of applications due to large local field enhancement that occurs in the vicinity of metal surface. Based on the quasi-static dipole approximation limit of Mie theory, a metallic nanoparticle sphere acts as a nanoantenna. In this paper, we studied the coupling between the excitons in the emission layer (MEH:PPV) and gold nanoantenna which is blended into the polymeric matrix (PEDOT:PSS) in a layer structure. Compared to the sample without Au particles mixing, surface plasmon resonance coupling to molecular excited state resulted in fluorescence enhancement of up to 2.3x in overall relative quantum efficiency. As the fluorescent emitters was in the vicinity of metal surface, the local field enhancement lead to a increased excitation probability whereas nonradiative energy transfer to particle result in a decrease of quantum yield. The phenomenon was discussed by changing the separation between gold nanoantenna and singlet polaron excitons to obtain the optimized quantum yield. In this study, the optimal thickness (thickness of spacer layer) was determined to be 30 nm. The structure can be utilized in most electroluminescent polymeric system. The results revel that the optical efficiency can be effectively enhanced without sacrificing the electric properties.

致　謝

　　首先要感謝我的指導教授田仲豪老師，在這兩年來不辭辛勞的教導我，提供很多關於實驗上的相關知識與建議，尤其是老師對於學問研究求知的態度更是我效法的對象，對於我的學業與實驗有著極大的幫助，並順利完成此論文。

　　再來我要感謝鄭璧如學姊和鄭榮安博士在理論和實驗上的協助，在研究過程中提供了許多寶貴意見和實驗所需資源，也讓我學到很多做人處事的道理。

　　在實驗室裡的日子裡，感謝健翔、進哥、Blue、小陸、阿誠、阿昇、貢丸、牛奶、董哥、展燁、小夫、筱儒、志宏，在課業上、生活上、研究上的分享，陪伴我一起度過這些快樂的日子。

　　最後感謝我的家人，感謝你們多年來的支持與鼓勵，在生活上細心照顧與關懷，讓我能無後顧之憂的研究與學習，並順利完成碩士學位。這份喜悅我將與幫助過我的各位分享。

Table of Contents

Figure Captions

Tables

Chapter 1

Introduction and Objective

1.1 History of nanoparticles

Nanotechnology, nanoscience, nanostructures or nanoparticles (NPs) are now some of the most widely used terms in materials science literature. But why are nanoscale materials and processes so attractive? Nanostructured materials have potential applications in many areas, such as biological detection, drug delivery, microscopy, optical devices, and sensors [1] [2] [3] [4]. In fact, metallic nanoparticle has been utilized as a colouring pigment dating back to the middle ages. The nanoparticles are embedded into the glass to form the famous Lycurgus Cup (4th century AD) (**Figure1-1**) [5]. The cup can still be seen at the British Museum and possesses the unique property of changing color depending upon the light in which it is viewed.

(a)
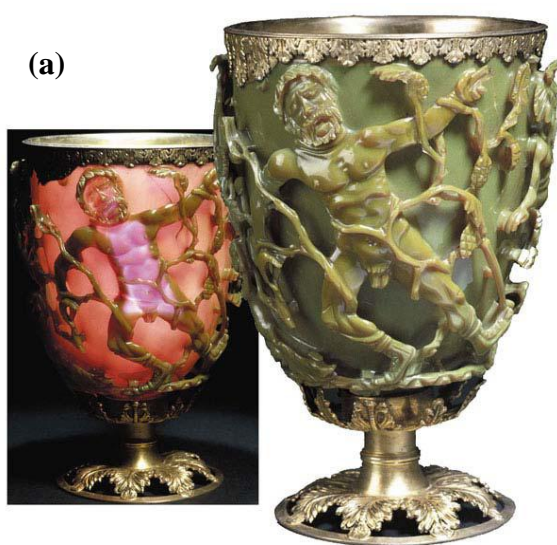
Figure 1-1(a) Lycurgus Cup, Roman Era (4th Century A.D). It appears green in reflected light and red in transmitted light. It contains gold and silver particles of approximately 70 nm **(b)** and in the molar ratio 1:14. The special color effect is due to these nanocrystals

(b)
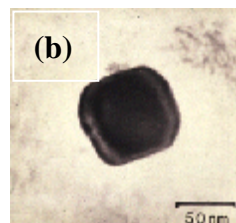
It appears green when viewed in reflected light, but looks ruby when the light is shone from inside and is transmitted through the glass. Analysis of the glass reveals that it contains a very small amount of tiny (~70 nm) metal crystals containing Ag and Au in an approximate molar ratio of 14:1. It is the presence of these nanocrystals that renders the Lycurgus Cup its colorful appearance. In the nineteenth, Faraday believed that the bright red color of the gold colloidal was due to the extremely small sizes of the individual particles, which interacted with light in a different manner compared to metallic gold, but could not prove it [6]. Mie in 1908 developed a complete theory of the scattering and absorption of electromagnetic radiation by a sphere, in order to understand the colors of colloidal gold particles [7]. Since that pioneering work, lots of papers have been published on the synthesis, modification, properties, and assembly of metal nanoparticles. At present, the desired size and shape of metallic nanoparticle can be prepared at a reliable procedure, and the physico-chemical properties have been understood deeply, helps us to determine the characteristic behavior of the built systems.
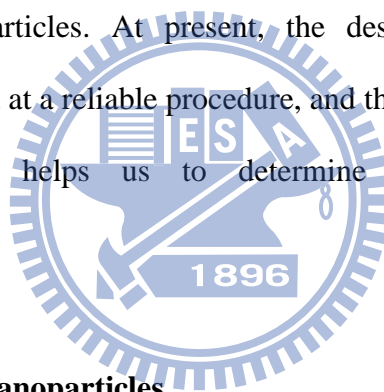
1.2 Optical Properties of Nanoparticles

As light interacts with metallic nanoparticles, it excites free electrons on the surface to result in collective electron density oscillation, which is called localized surface plasmon. This resonant plasmon is sensitive to the shape and size of the nanoparticles. For noble metals with free electrons (Au, Ag, Cu, and the alkali metals), which have plasmon resonances at the visible spectrum, which give rise to such vivid colors. Bulk Au looks yellowish in reflected light, but thin Au films look blue in transmission. As the particle size is reduced down to ~3 nm, the color tends gradually to orange, through several tones of purple and red. Elongated nanoparticles (ellipsoids and nanorods) display two distinct plasmon bands related to transverse and longitudinal electron oscillations. The longitudinal oscillation is very sensitive

to the aspect ratio of the particles, so that slight deviations from spherical geometry can lead
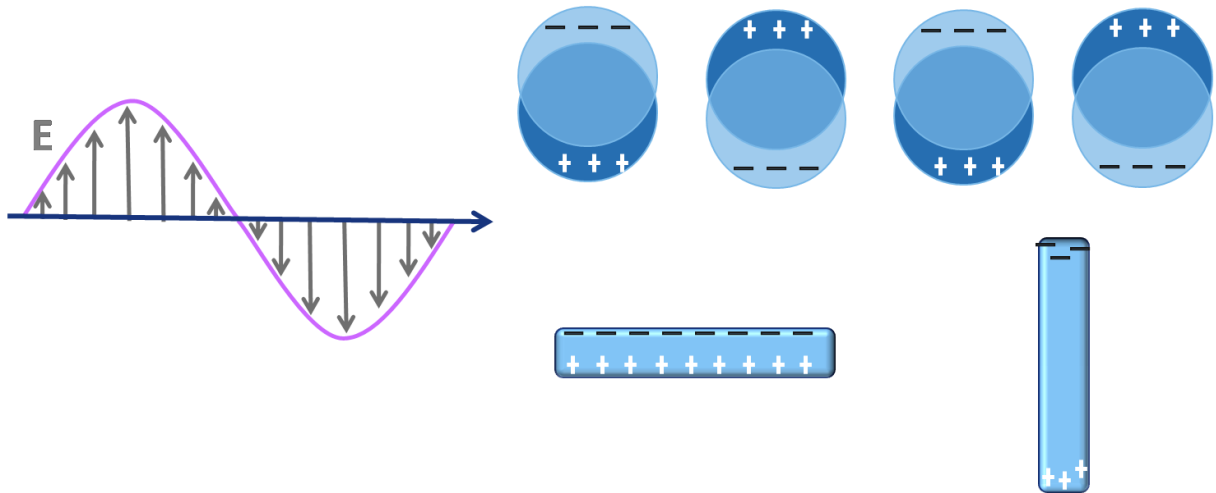
Figure 1-2 (**Top**) Schematic drawing of the interaction of an electromagnetic radiation with a metal nanosphere. A dipole is induced, which oscillates in phase with the electric field of the incoming light. (**Bottom**) Transverse and longitudinal oscillation of electrons in a metal nanorod

to impressive color changes [8]. As **Figure 1-2** shows, the electric field of the incoming light induces the formation of a dipole in the nanoparticle. A restoring force in the nanoparticle tries to compensate for this, resulting in a specific resonance wavelength (**Figure 1-2, top**). The oscillation wavelength depends on a number of factors, including particle size shape, the surrounding medium, and so on. For nonspherical particles, such as rods, the resonance wavelength depends on the orientation of the electric field. Therefore, two oscillations, transverse and longitudinal, are possible (**Figure 1- 2, bottom**) [9]. In addition, when nanoparticles are sufficiently close together, interactions between adjacent particles arise, so that the models for isolated particles do not hold. The properties of dilute dispersions will be briefly discussed first. In the section 2, the Mie theory of dilute dispersion will be discussed deeply to understand the optical properties of spherical Au nanoparticle in the quasic-static approximation.

1.3 Motivation

Engineering the spectral properties of fluorophores, such as the enhancement of

luminescence intensity, can be achieved through coupling with surface plasmons in metallic nanostructures [3]. Some of the approaches have relied upon the coupling of fluorophores (typically organic dyes) to random distributions of metallic nanoparticles or nanoscale roughness in metallic films [10]. This process, referred to as metal-enhanced fluorescence, offers promise for a range of applications, including LEDs, sensor technology, microarrays and single-molecule studies. The technique of metal enhanced fluorescence (MEF) is based upon the design of metallic surfaces in the vicinity of the emitter. MEF yields an overall improvement in the fluorescence detection efficiency through modification and control of the local electromagnetic environment of the emitter. Near-field coupling between the emitter and surface modes plays a crucial role in MEF. Besides, it becomes even more appealing when applied to nanoparticle (NPs), which exhibit size and spatially dependent optical properties and are characterized by broad surface plasmon absorption spectra.

In 1946 Purcell suggested that spontaneous emission of molecules could be modified by a resonant coupling with an external electromagnetic field [11]. Such kind of environmental condition could be observed near noble metal surfaces and nanoparticles due to localized surface plasmon (LSP) which confines the incident light into the near field to give rise to a great enhancement of the local electromagnetic field. Since then, many studies pointed out that combining metallic nanostructures with molecules lead to a modification of the molecular fluorescence [1] [2]. Experimental and calculation results pointed out that both molecular absorption and emission processes are modified by LSP. In case of absorption, the electromagnetic field enhancement increases the absorption transition probability for molecules near nanoparticles, leading to an increase of the molecular fluorescence intensity. On the other hand, the fluorescence emission process is more complex. LSP could modify both radiative and nonradiative molecular transition results in enhancement and quenching, respectively.

1.4 Objective
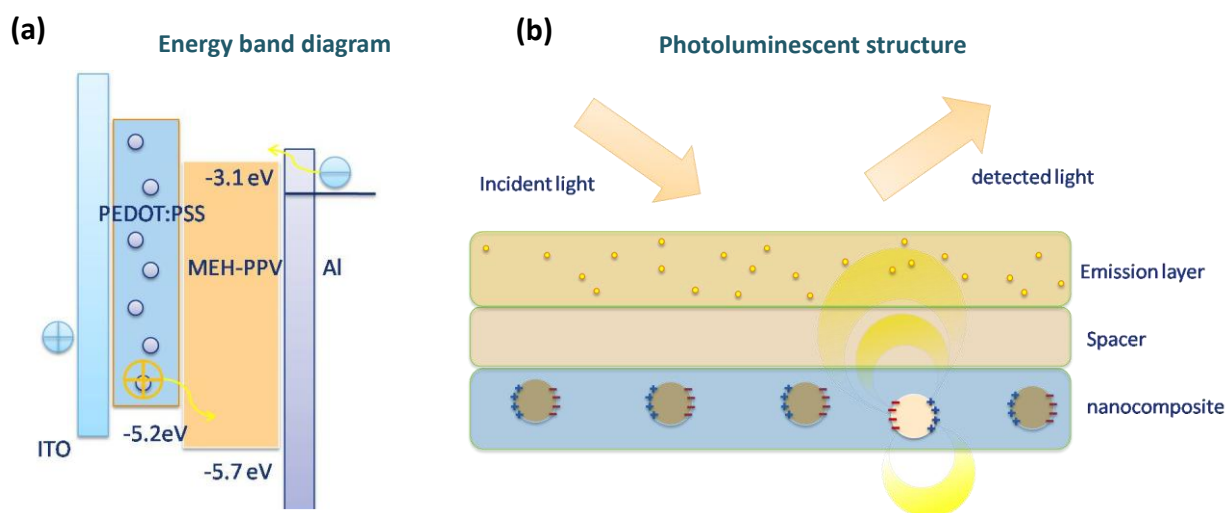
Figure 1-3 (a) In a conventional polymer based light-emitting diode, PEDOT:PSS play a role as hole-injection layer to reduce hole energy barrier. Here, we introduce Au nanoparticles into PEDOT:PSS layer to mediate the luminescence and spectral behavior of light-emitting polymer. Without sacrifice of electronic properties, this material was adopted to investigate the optical properties of localized surface plasmon coupled photoluminescent engineering.

(b) The nanoparticle (~92nm) behaves as a nanoantenna. Here we studied the coupling of the excitons in the emission layer (MEH:PPV) to gold nanoantenna which is blended into the polymeric matrix (PEDOT:PSS). The Au NPs are dilute enough (surface density ~1%) so that the interaction between NPs are beyond the scope of this research. A spacer layer was inserted to modify the fluorescence quantum yield of emission layer. At this time, the interaction between excitons in emission layer and one Au NP can be considerate.

Some papers mentioned that metals are notorious for quenching the radiation of emitters placed in their near field. On the other hand, it is known that luminescence can be enhanced on metallic nanostructures. The desire to understand and exploit these phenomena has triggered a large number of investigations [3] [12] [13]. However, quantitative measurement and comparisons with theoretical predictions have been plagued by the lack of control over the parameter that determines the radiation properties of emitters close to the metallic nanostructure. And the research is rarely observed in lectures on metal mediated spectral

design in an electroluminescent polymeric system. To address this challenging these issues, we have studied the interaction of fluorescent polymer with spherical gold NPs under separation control in a light emitting polymeric system. Here, we proposed here a new strategy based on the highly reproducible preparation of light emitting polymers coupled with Au nanoparticles dispersed in a polymer matrix. The possibility in this semiconducting polymeric architecture was in addition demonstrated of obtaining the high quantum efficiency and spectral engineering from PL (photo-luminescence) enhancement process. Furthermore, the randomly dispersed gold nanoparticles film was uniquely prepared in a nano-form of semiconducting polymer and metal nanoparticle composites or the so-called nanocomposites layer [14] [15]. Of the major semiconducting polymers, poly(3,4-ethylenedioxy-thiophene)/poly(styrene)-sulfonate (PEDOT:PSS) has proven intriguing particularly due to its optical transparency in its conducting state, as well as the role as a hole-injection layer to reduce the energy barrier between the active layer and the anode layer (*Figure 1-3 (a)*). So in this work, hydrophilic PEDOT: PSS was chosen to be solution processed and then mixed with gold nanoparticles to compose the nanocomposite material [16] [17]. Without deterioration of electronic properties [18], this material was inserted to investigate the physical and optical properties of surface plasmon coupled PL engineering, as shown in **Figure 1-3(b)**. Furthermore, spherical Au nanoparticle in the quasic-static approximation acts as a nanoantenna. And inserting a spacer layer (PEDOT:PSS) can tune the distances of resonant coupling between nanoantenna in the NC and excitons in emission layer. In practice, the design with desired parameters will be realized in a polymeric optoelectronic device which is very attractive for versatile potential applications like polymer light-emitting diodes (PLEDs). Similar scheme has been realized in electroluminescence of small emissive organic molecules interacted with quantum-sized (diameter<10 nm) NPs-incorporated NC by Ha's group [19]

Chapter 2

Theory

2.1 Localized Surface Plasmons

Localized surface plasmons are non-propagating excitations of the conduction electrons of metallic nanostructures coupled to the electromagnetic field. For a nanoparticle, the dipole
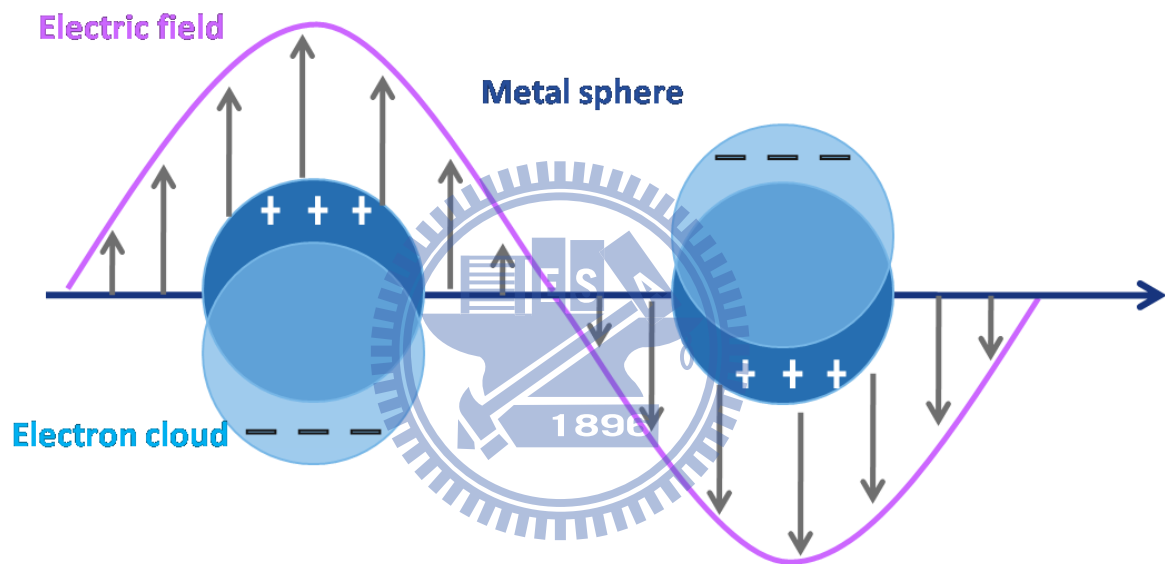
Figure 2-1 Schematic of plasmon oscillation for a nanoparticle

created by electric field **(Figure 2-1)** leading to the net charge difference on the surface. These charges act as an effective restoring force, which allows a specific wavelength to occur resonance. The resonance called the localized surface plasmon results in field amplification both inside and in the near-field zone outside the particle [8]. Another consequence of the spherical nanoparticles is that plasmon resonances can be excited by direct light illumination, in contrast to propagating SPPs. (surface plasmon polaritons)

Incident light interacts strongly with metallic colloids at resonance wavelength. This property is shown in **Figure 2-2** where a metallic nanoparticle with size *a* is illuminated with light (λ) **(Figure 2-2 bottom)** and a wavelength at the plasmon resonance at λ_p **(Figure 2-2 top)** [20]. The crooked lines represent the energy flow near the particle. In this case, the metallic nanoparticle presents an optical cross-section D_1 much greater than its physical cross-section d. This effect is seen by the energy flow into the particle, which results in the enhanced fields around illuminated nanoparticles. For λ ($\lambda > \lambda_p$), the optical cross section D_2 can be smaller than physical cross section d (bottom) .

For noble nanoparticles (Au, Ag, and Cu), the resonance falls into the visible region of the electronmagnetic spectrum. A consequence of this is that the particles shows the bright colors both in transmitted and reflected light, due to enhanced absorption and scattering at resonant wavelength. This effect has found applications for many hundreds of years, for example in the staining of glass for windows or ornamental cups.
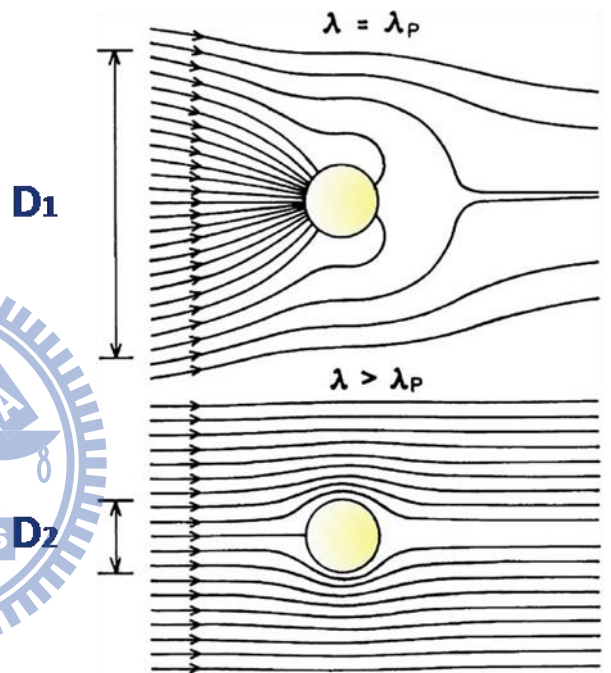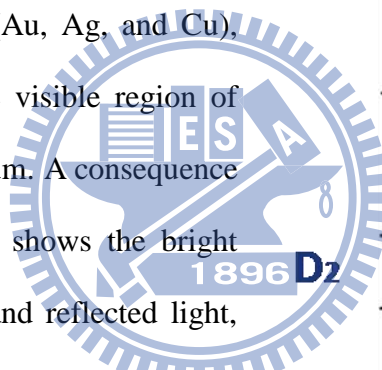
Figure 2-2 Energy flow (crooked lines) near a subwavelength metallic nanoparticle with diameter *a* illuminated at the resonant wavelength (top) and at a wavelength longer than the wavelength (bottom). The vertical lines on the left show optical cross-sections for absorption.

2.2 Mie Theory

The theory of scattering and absorption of radiation by a small sphere predicts a resonant field enhancement due to a resonance of the polarizability α if the Fröhlich condition is

satisfied. Under these circumstances, the nanoparticle acts as an electric dipole **(Figure 2-3)**, resonantly absorbing and scattering electromagnetic fields. This theory of the dipole particle plasmon resonance is strictly valid only for extremely small particles. In practice, the calculations in the following section provide a reasonably good approximation for spherical particles with dimensions below 100 nm illuminated with visible or near-infrared radiation.

However, for larger dimension, where the quasi-static approximation is no longer valid due to significant phase-changes of the driving field over the particle volume, a rigorous electrodynamic approach is required. Mie in 1908 developed a complete theory of the scattering and absorption of electromagnetic radiation by a sphere, in order to understand the colors of colloidal gold particles. Mie theory is the approach to expand the internal and scattered fields into a set of normal modes described by vector harmonics. The quasi-static results valid for sub-wavelength spheres are then recovered by a power series expansion of the absorption and scattering coefficients and retaining only the first term.
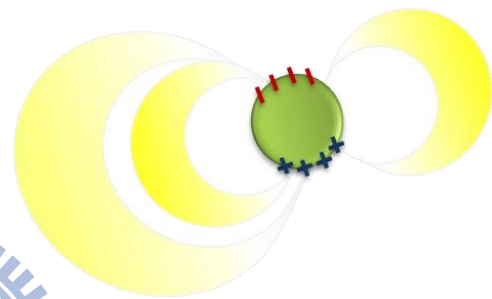
Figure 2-3 The scattering properties and the plasmon spectra of small gold nanoparticles are well described in the quasistatic dipole approximation limit of Mie theory. Thus, given a dipolar radiation pattern and a well-defined resonance spectrum, a gold nanoparticle behaves as an elementary resonant dipole antenna.

Since Mie theory is discussed in a variety of textbooks [8][20] and a detailed knowledge of the higher order terms is not required for our purpose. Alternatively, we will merely examine the physical consequences of the first-order corrections to the quasi-static approximation.

2.2.1 Normal Modes of Sub-Wavelength Metallic Particles

The interaction of a particle of size *a* with the electromagnetic field can be analyzed using

the simple quasi-static approximation provided that $a \ll \lambda$, the particle is much smaller than the wavelength of light in the surrounding medium. In this case, the phase of the harmonically oscillating electromagnetic field is practically constant over the particle volume, so that one can calculate the spatial field distribution by assuming the simplified problem of a particle in electrostatic field. The harmonic time dependence can then be added to the solution once the field distributions are known. This lowest-order approximation of the full scattering problem describes the optical properties of nanoparticles of dimensions below 100 nm adequately for many purposes.

In the following discussion, a homogeneous, isotropic sphere of radius a located at the origin in a uniform, static electric field $\mathbf{E} = E_0 \hat{\mathbf{z}}$ will be analyzed (**Figure 2-4**). The
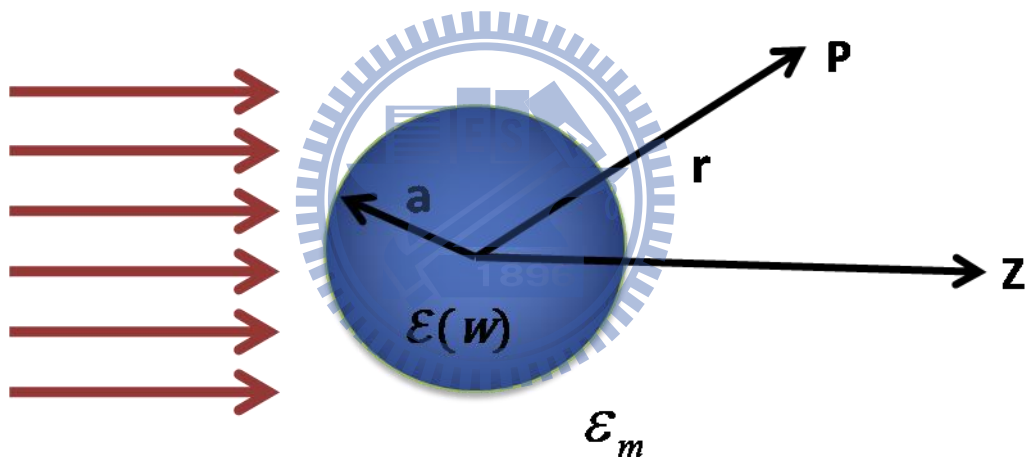
Figure 2-4 Sketch of a homogeneous sphere placed into an electrostatic field.

surrounding medium is isotropic and non-absorbing with dielectric constant ε_m, and the field lines are parallel to the z-direction. The dielectric of the sphere $\varepsilon(w)$ depends on the frequency of incident light.

In the electrostatic approach, we are interested the potential at the position r at the point P, so that we can get obtain the electric field by calculating $\mathbf{E} = -\nabla \Phi$. By solving the Laplace

equation $\nabla^2 \Phi = 0$, the general form of the potential is

$$\Phi(r, \theta) = \sum_{\ell=0}^{\infty} \left[A_\ell r^\ell + B_\ell r^{-(\ell+1)} \right] P_{\ell(\cos \theta)} \ , \tag{2-1}$$

Where $P_{\ell(\cos \theta)}$ are the Legendre Polynomials of order ℓ, and θ indicates the angle between the position vector **r** at the point **P** and the z-axis. Due to the requirement that the potentials remain finite at the origin, the solution for the potentials Φ_{in} inside and Φ_{out} outside the sphere can be written as

$$\Phi_{in} = \sum_{\ell=0}^{\infty} A_\ell r^\ell \, P_{\ell(\cos \theta)} \tag{2-1a}$$

$$\Phi_{out} = \sum_{\ell=0}^{\infty} \left[B_\ell r^\ell + C_\ell r^{-(\ell+1)} \right] P_{\ell(\cos \theta)}. \tag{2-2b}$$

Now we can determine the coefficients A_ℓ, B_ℓ from the boundary conditions at $r \to \infty$ and at the sphere surface $r = a$. At infinite position ($r \to \infty$), the requirement that $\Phi_{out} \to -E_0 z \to -E_0 r \cos \theta$ demands that $B_1 = -E_0$ and $B_\ell = 0$ for $\ell \neq 1$. The remaining coefficients A_ℓ and C_ℓ are defined by the boundary conditions at $r = a$.

$$\Phi_{out}(a, \theta) = \Phi_{in}(a, \theta) \tag{2-3}$$

$$\varepsilon E_{in} \hat{n} = \varepsilon_m E_{out} \hat{n} \tag{2-4}$$

Application of these boundary conditions leads to $A_\ell = C_\ell = 0$ for $\ell \neq 1$, and via the calculation of the remaining coefficients A_ℓ and C_ℓ the potentials evaluate to

$$\Phi_{in} = -\frac{3\varepsilon_m}{\varepsilon + \varepsilon_m} E_0 r \cos \theta \tag{2-5a}$$

$$\Phi_{out} = -E_0 r \cos \theta + \frac{\varepsilon - \varepsilon_m}{\varepsilon + 2\varepsilon_m} E_0 a^3 \frac{\cos \theta}{r^2}. \tag{3-5b}$$

Φ_{out} describes the superposition of applied field and the field created by a dipole located at the particle center. We can rewrite Φ_{out} by introducing the dipole moment **p** as

$$\Phi_{out} = -E_0 r \cos\theta + \frac{\mathbf{p}\cdot\mathbf{r}}{4\pi\varepsilon_0\varepsilon_m r^3} \qquad \text{(2-6a)}$$

$$\mathbf{p} = 4\pi\varepsilon_0\varepsilon_m a^3 \frac{\varepsilon-\varepsilon_m}{\varepsilon+2\varepsilon_m}\boldsymbol{E_0} \qquad \text{(2-6b)}$$

The applied field induces a dipole moment inside the sphere of magnetic proportional to $|E_0|$. If we introduce the polarizability α, defined via $\mathbf{p} = \varepsilon_0\varepsilon_m\alpha\boldsymbol{E_0}$, we obtain

$$\alpha = 4\pi a^3 \frac{\varepsilon-\varepsilon_m}{\varepsilon+2\varepsilon_m} \qquad \text{(2-7)}$$

Equation **(2-7)** is the center result of this section, the (complex) polarizability of a small sphere of sub-wavelength diameter in the electrostatic approximation. When the value of $|\varepsilon + 2\varepsilon_m|$ is a minimum, the polarizability experiences a resonant enhancement. For the case of small or slowly-varying $\text{Im}[\varepsilon]$ around the resonance, the minimum of $|\varepsilon + 2\varepsilon_m|$ can be simplifies to

$$\text{Re}[\varepsilon(w)] = -2\varepsilon_m \qquad \text{(2-8)}$$

This relationship is called the Fröhlich condition and the dipole surface plasmon of the metal nanoparticle. For a sphere consisting of a Drude metal with a dielectric function

$$\varepsilon(w) = 1 - \frac{w_p^2}{w^2 + i\gamma w}$$

located in air, the Fröhlich condition is met at the frequency $w_0 = w_p/\sqrt{3}$. Equation **(2-8)** further expresses the strong dependence of the resonance frequency on the dielectric environment：The resonance red-shifts as ε_m is increased. Metal nanoparticles are thus ideal platforms for optical sensing of changes in refractive index.

The electric field $\mathbf{E} = -\nabla\Phi$ can be obtained from the potentials (**2-5**)

$$\mathbf{E_{in}} = -\frac{3\varepsilon_m}{\varepsilon + 2\varepsilon_m}\mathbf{E_0} \tag{2-9a}$$

$$\mathbf{E_{out}} = \mathbf{E_0} + \frac{3\mathbf{n}(\mathbf{p}\cdot\mathbf{r}) - \mathbf{p}}{4\pi\varepsilon_0\varepsilon_m}\frac{1}{r^3}. \tag{2-9b}$$

The resonance in α also implicates a resonant enhancement of both the internal and dipolar fields. It is this field-enhancement at the plasmon resonance on which many of the prominent applications of metal nanoparticles in optical devices and sensors rely.

2.2.2 Fields Induced by Oscillating Dipole

The basics of the electromagnetic fields associated with an oscillating electric dipole. The total fields $\mathbf{H}(t) = \mathbf{H}e^{-i\omega t}$ and $\mathbf{E}(t) = \mathbf{E}e^{-i\omega t}$ in the near, intermediate zones of a dipole can be written as

$$\mathbf{H} = \frac{ck^2}{4\pi}(\mathbf{n}\times\mathbf{p})\frac{e^{ikr}}{r}\left(1 - \frac{1}{ikr}\right) \tag{2-10a}$$

$$\mathbf{E} = \frac{1}{4\pi\varepsilon_0\varepsilon_m}\left\{[3\mathbf{n}(\mathbf{p}\cdot\mathbf{r}) - \mathbf{p}]\left(\frac{1}{r^3} - \frac{ik}{r^2}\right)e^{ikr} + k^2(\mathbf{n}\times\mathbf{p})\times\mathbf{n}\frac{e^{ikr}}{r}\right\} \tag{2-10b}$$

with $k = \frac{2\pi}{\lambda}$ and $\mathbf{n}$ unit vector in the direction of point **P**. The term in **2-10b** decayed as r^{-3} is called the static field, and the one decayed as r^{-2} is called the induction field. The last term decayed as r^{-1} is called radiation field. Only the radiation field can propagate to infinite distance which can be seen as the far-field component; the other two are the near-field components.

In the near zone ($kr \ll 1$), the electrostatic result **(2-9b)** for the electric field is recovered. The

static field is dominant and $|E| \propto \left(\frac{1}{r}\right)^3$

In the opposite limit of radiation zone, defined by $kr \gg 1$, the dipole fields are of the spherical-wave form

$$H = \frac{ck^2}{4\pi}(\mathbf{n} \times \mathbf{p})\frac{e^{ikr}}{r} \qquad \textbf{2-11a}$$

$$E = \sqrt{\frac{\mu_0}{\varepsilon_0 \varepsilon_m}}(\mathbf{H} \times \mathbf{n}). \qquad \textbf{2-11b}$$

2.2.3 Scattering Cross Section

From the viewpoint of optics, it is more interesting to note that another consequence of resonantly enhanced polarization α implies the efficiency with which a metal nanoparticle scatters and absorbs light. The corresponding cross sections for scattering and absorption C_{sca} and C_{abs} can be calculated via the Poynting-vector determined from **(2-10)** to

$$C_{sca} = \frac{k^4}{6\pi}|\alpha|^2 = \frac{8\pi}{3}k^4a^6\left|\frac{\varepsilon - \varepsilon_m}{\varepsilon + 2\varepsilon_m}\right|^2 \qquad \textbf{2-12a}$$

$$C_{abs} = k\,\text{Im}[\alpha] = 4\pi ka^3\text{Im}\left[\frac{\varepsilon - \varepsilon_m}{\varepsilon + 2\varepsilon_m}\right] \qquad \textbf{2-12b}$$

For small particles with $a \ll \lambda$, the efficiency of absorption, scaling with a^3, dominates over the scattering efficiency, which scales with a^6. Equations **(2-12)** also shows that when the Fröhlich condition **(2-8)** is met, both absorption and scattering for the metallic particle are resonantly enhanced at the dipole particle plasmon resonance. For a sphere of volume V and dielectric function $\varepsilon = \varepsilon_1 + i\varepsilon_2$ in quasi-static limit, the explicit expression for the extinction cross section $C_{ext} = C_{abs} + C_{sca}$ can be written as

$$C_{\text{ext}} = 9\frac{w}{c}\varepsilon_m^{3/2}V\frac{\varepsilon_2}{[\varepsilon_1+2\varepsilon_m]^2+\varepsilon_2^2} \qquad \textbf{2-13}$$

2.3 Mental Enhancement Fluorescence

Fluorescence detection is the basis of many measurements in biological research, and it provides numerous measurement opportunities including studies of biological macromolecules, cell imaging, and DNA sequencing. In our research, we investigate the fluorescence quantum yield of MEH-PPV of its separation from a light irradiated, spherical gold nanoparticle. Our approach based on the use of gold nanoantennas is promising for various applications such as enhancement of weakly fluorescing systems.

From section **2.2.1**, **2.2.2**, the spherical nanoparticle acts as an electric dipole when the particle size is much smaller than the wavelength of light in the surrounding medium ($d \ll \lambda$), and as a light is irradiated on the particle, the electric field **E** is described by equation **(2-10b)**. To consider a single molecule located at $\mathbf{r}_m$ and represented by a three-level system with transition dipole moment **p** and transition frequency ω. The extrinsic quantum yield (Q.Y) can be represented as a three-level process which involves the excitation probability η_{exc} and the intrinsic quantum yield (emission decay rate ratio) $\eta_{\text{em}} = {\gamma_r}/{\gamma}$, with γ_r and γ being the radiative decay rate and the total decay rate, respectively **(Figure 2-5)**. The extrinsic quantum yield can then be written as

$$Q.Y = \frac{\text{number of radiative photons}}{\text{number of incident photons}} = \eta_{\text{exc}} \cdot \eta_{\text{em}} = \eta_{\text{exc}} \cdot \frac{\gamma_r}{\gamma_r+\gamma_{\text{nr}}} \qquad \textbf{(2-14)}$$

where $\gamma_{\text{nr}} = \gamma - \gamma_r$ is the nonradiative decay rate and $\eta_{\text{exc}} \propto |\mathbf{E}(\mathbf{r}_m,\omega)|^2$ is the excitation rate depending on the total local excitation field $\mathbf{E}(\mathbf{r}_m,\omega)$ (incident plus scattered) [21][22].
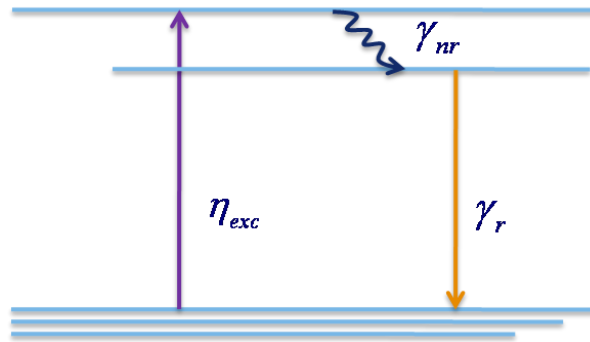
Figure 2-5 Sketch of a molecule represented as a three-level system

From equation **(2-14)**, the fluorescence is the product of two processes：(1) Excitation by the incident field which was influenced by the local environment, and (2) emission of radiation influenced by the balance of radiative and nonradiative decay. The source of process (1) is the external radiation field, and in process (2) it is the molecule itself which makes up the source.

Based on the pioneering work by Purcell, the emission rate of excited molecule depends not only its life time but also of the environment. It was realized that the modification of the life time is influenced by the radiative decay rate due to photon emission and by the irradiative decay rate due to energy dissipation in the
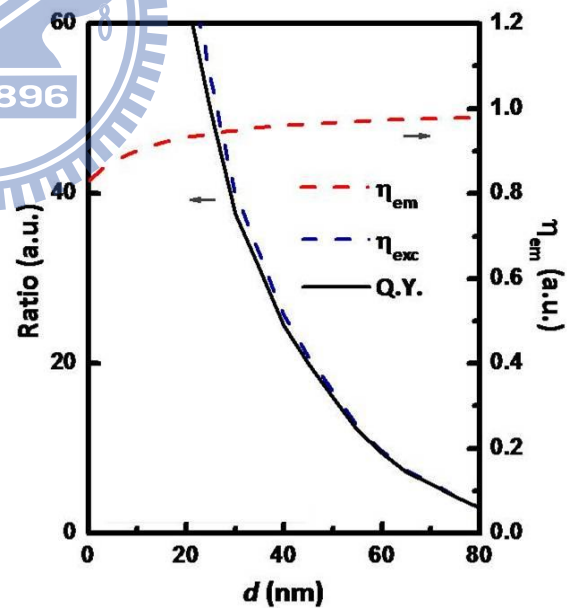
Figure 2-6 Nanoantenna enhanced quantum efficiency by exact electrodynamical method

environment. For atoms or molecules close to metal surfaces both rates can be enhancement. Excited-state lifetimes of single molecules have been measured as a function of their separation from light-irradiated metal boundaries and satisfactory agreement with theory has been achieved. However, previous experiments showed either fluorescence enhancement or fluorescence quenching. The problem originates that the competing effects between local field enhancement leads to an increased excitation probability and nonradiative energy transfer to the particle leads to a decrease of the quantum yield (quenching). The competing factors can be taken into accounts by the equation **(2-14)**, η_{exc}, γ_r, and γ_{nr} .By the exact electrodynamical method at the dipole approximation, the relative factors (η_{exc}, η_{em}) corresponded to quantum yield **(Equation 2-14)** was shown in **Figure 2-6**, which is plotted by exact electrodynamical.

Chapter 3

Experiment

3.1 Introduction

In order to see how the LSP modifies the spectroscopic properties of fluorescent polymer, we deposited an layer structure containing Au NPs (~92 nm diameter) dispersed in PEDOT:PSS as the solvent, and a layer (100 nm thickness) of MEH-PPV play a role of active layer. The separation (deposited with PEDOT:PSS) between gold nanoparticle and emission layer can be altered to obtain an optimal quantum yield. For discussing photoluminescence, the unpolarized light with specific wavelength (depends on the peak of absorption spectrum of individual sample) is incident into samples on the side of emission layer. And the detector is on the same side of the incident light with the same incident angle to the normal of the sample. An important advantage of this polymeric system is not only the photoluminescence can be discussed but also electrolumiscence does, when the structure (**Figure 1-3**) is sandwiched by the ITO (Indium Tin Oxide) layer (anode) and aluminum layer (cathode). Once the voltage is applied to electrodes, the electrolumiscence can be discussed. At this time, nanocomposite layer functions as not only a hole-injection layer but also a metallic nanostructure layer.

We propose not only a simple way but also a stable technology to fit the ideal experimental structure we designed (layer-by-layer structure). That is the spin-coating fabrication **(Figure 3-1)**. It provides a convenient step-by-step method for precise and uniform deposition of thin films and coating, and the materials including polymer or nanocomposite can be easily deposited on quartz or ITO substrates. At the following parts, the detail experimental-process will be presented step by step.
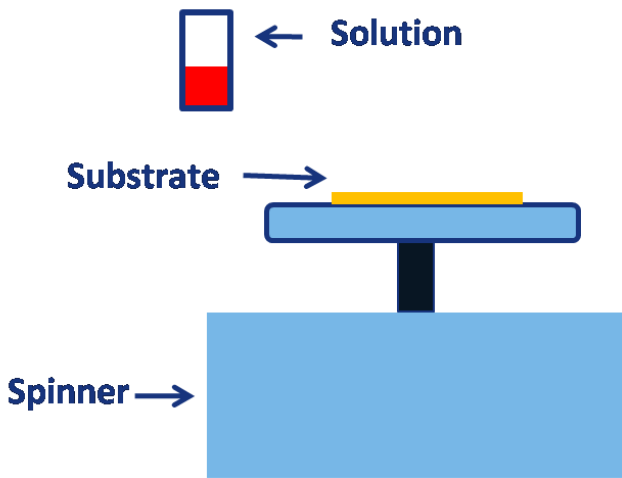
Figure 3-1 Spin coating is an economical and fast method to produce homogeneous layers. An excess amount of the solvent is placed on the substrate, which is then rotated at high speed by spinner in order to spread the fluid by centrifugal force. The film thickness can be adjusted by varying the rotation speed, the rotation time, and the concentration of the used solution.

3.2 Fabrication Flow

In our research, we investigate the fluorescence quantum yield of MEH-PPV of its
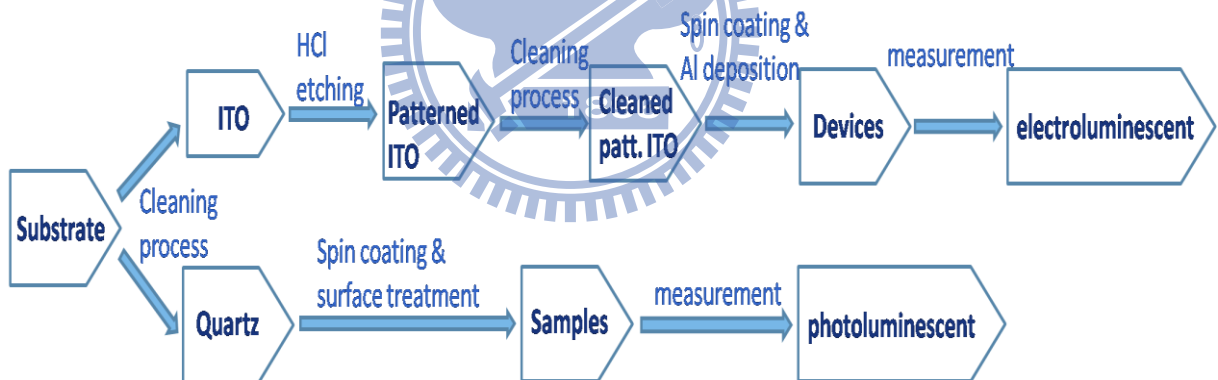
Figure 3-2 Fabrication flow for optical and electrical measurement

separation from a light irradiated, spherical gold nanoparticles. However, in our system, once the fluorescence is discussed, the measurement of photoluminescent (PL) and electroluminescent (EL) are good ways to examined. We presented a feasible experimental process of fabricating the samples for optical measurement (PL) and devices for electrical measurement (EL). For the electroluminescent measurement, the ITO substrate has to be

patterned, cleaned, and layer deposited sequentially, and in the final the device is finished to be measured. For the photoluminescent measurement, the electrodes of metal deposition can be ignored. After cleaning the quartz substrate and depositing polymer layers sequentially, the samples for photoluminescence measurement is completed. The **Figure 3-2** shows the fabrication flow.

3.2.1 Cleaned ITO & Quartz Substrate and Surface Treatment

ITO or Quartz substrate (GE214/124) was sequentially cleaned in the acetone, detergent ,and DI water each for 40min with an ultrasonic cleaner, and then baked at 140℃ for 1hr. Before spin coating PEDOT: PSS layer, not only ITO but also Quartz substrate has to be UV-ozone treated for 10min. The UV-ozone treats the surface to remove the organic or oxygen residues and showing a good wetting property before PEDOT:PSS film coating.

3.2.2 Preparation of Gold Nanoparticle Solution

Spherical Au NPs with various sizes were synthesized in ambient atmosphere by a chemical reduction. [23]Due to the fact that concentration and various sizes have crucial influence over absorption and scattering properties of gold NPs, a conclusive gold NP parameter over sizes and
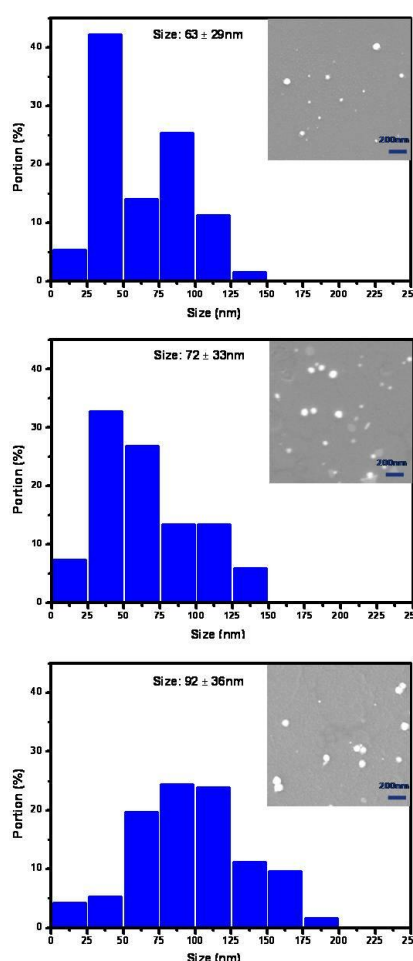
Figure 3-3 Size distributions. Insets show SEM images.

concentration would be decided. 3 different average size of Au nanoparticles distribution 63±29, 72±33 and 92±36 nm were synthesized. **Figure 3-3** shows the particles size distributions of synthesized Au NPs as a function of reaction time. Inset shows SEM images.

3.2.3 Preparation of PEDOT:PSS-Au Nanocomposite & MEH-PPV

PEDOT:PSS (Baytron® . P， Al 4083) has been widely adopted as a hole injection material in achieving highly efficient PLED. As it forms layer structure by spin-coating, the layer is a transparent and conductive polymer. It both flattens the surface and matches the work function of the anode of the device. Before making use of PEDOT:PSS solution, it must be filtered through a 0.22 um membrance filter (PVDF). 10 w.t. % hybrid PEDOT:PSS-Au nanocomposite solutions were prepared and then to be put into an ultrasonic bath for 30 min. MEH-PPV is conjugated, hole-transporting polymer. In this research, it is prepared for 0.8 w.t. % using toluene as solvent. The molecule structure of PEDOT:PSS and MEH-PPV are shown in **Figure 3-4(a)** and **(b)**, respectively.
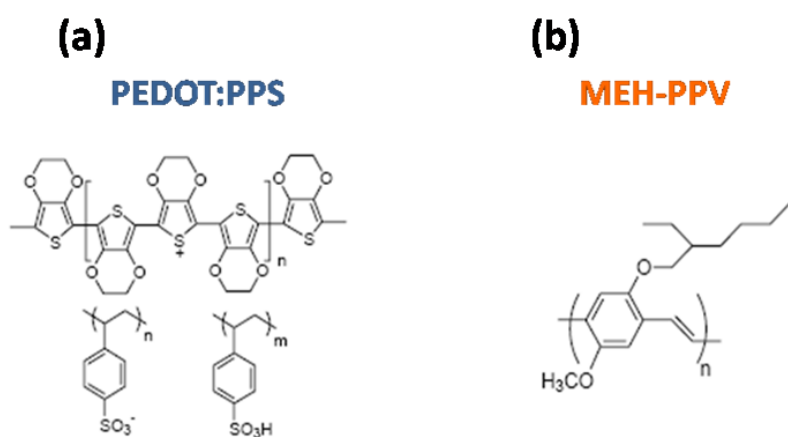
Figure 3-4 Molecular structure of (a) PEDOT:PSS (b) MEH-PPV.

3.2.4 Preparation of Samples

After cleaning process on quartz substrate, the PEDOT:PSS-Au nanocomposite solution was spin-coated at 2000 rpm onto the cleaned ITO/quartz substrates, and then baked at 140℃ for 1 hr. Spacer layer (PEDOT:PSS) with various thickness was subsequently spin-coated on the nanocomposite layer. In the final, the emitting layer (MEHPPV) with the thickness of 100 nm was deposited on top of the spacer layer. **Figure 3-5** shows the structure.
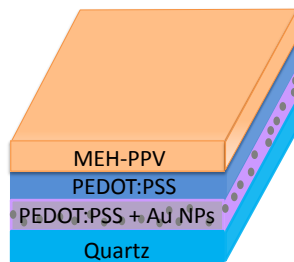
Figure 3-5 The cross-section of sample

3.2.5 Patterning ITO/quartz substrate

ITO (Indium Tin Oxide) is a transparent conducting material. It is always coated on the quartz substrate. Before fabricating devices, ITO must be patterned for defining efficient emitting area. A general patterning flow is shown in **Figure 3-6**.

At first, the tapes are applied to ITO substrate where we want to retain. This substrate is then put into shallow container filled with HCl

Patterning by tapes

Etching ITO by HCl

Peeling off the tapes
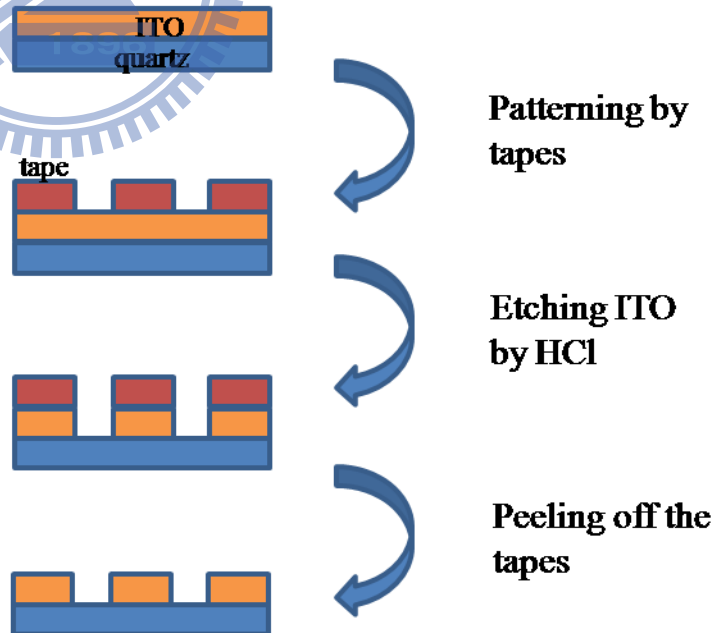
Figure 3-6 Schematic description of pattering ITO/quartz substrate.

liquid for 2min at 70℃, and sequentially to put the substrate into the container filled with D.I. water as fast as possibile for rinsing out the residual HCl. The parts which are mantled by tapes will be left, the others will be etched off by HCl liquid. In the final, using the tweezer to pick up the residual tapes, and a patterned ITO/quartz is finished. **Figure 3-7** shows the ITO substrate after patterening.
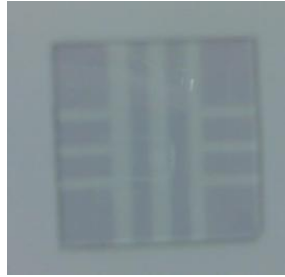
Figure 3-7 The patterning ITO/quartz substrate which we design.

3.2.6 Device Fabrication

The various thickness of device structures, ITO/PEDOT:PSS-Au/ PEDOT:PSS (spacer) /MEH-PPV/Al, were prepared in the following manner for EL measurement. For all structures, the patterned indium-tin-oxide quartz substrates were cleaned ultrasonically with acetone, detergent ,and DI water each for 40min. After cleaning, 10% hybrid PEDOT:PSS-Au nanocomposite solutions was spin-coated at 2000 rpm onto the cleaned ITO substrates and baked at 110 ℃ for 4 h. Spacer layer (PEDOT: PSS) were subsequently spin-coated on the PEDOT-Au nanocomposite layer; a 100-nm layer of emission layer (MEH-PPV) were sequentially deposited. For applying the voltage to active areas, the rest parts of ITO have to be rinsed. After spin coating each layer on quartz, the sample must be cleaned with individual solvent to remove the polymer layer almost everywhere from the sample, except for the middle region that the active areas located at. And then the samples are attached to a designed

mask to deposit a layer of Al. Like **Figure 3-9** shows. The battle used as a insulator for isolating each emission area. The emitting area of the device was defined as 3 mm _ 3 mm.
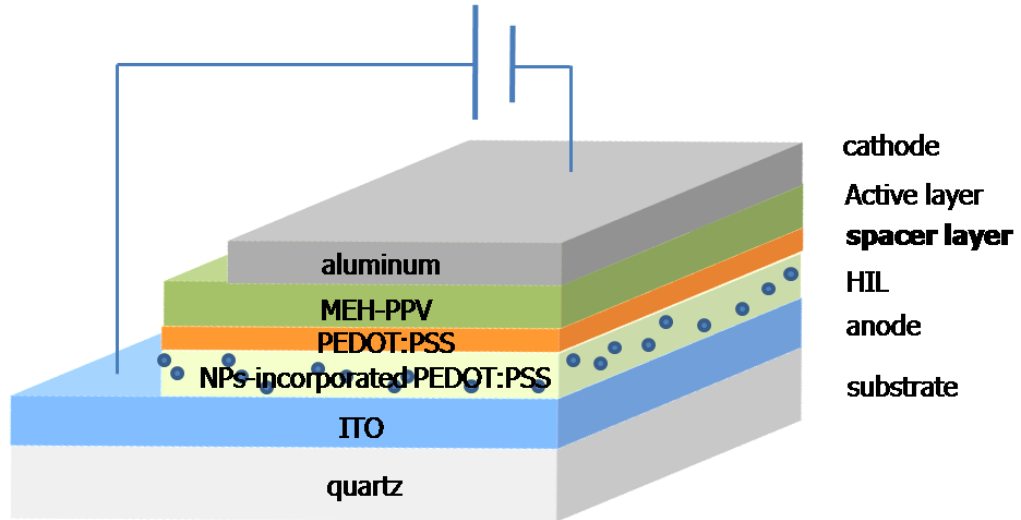
Figure 3-8 The cross-section of the device and the functions of each layer.

3.2.7 Package

After depositing the cathode, we package the sample with a smaller piece of glass in the glove box under nitrogen environment. The package processes includes applying the transparent UV-curably glue around the small glass, covering it on our sample and finally expose it to UV-light for 40 seconds. After exposure, the UV-curable adhesive holds together the glass and quartz, so that the active layers between them are protected well.
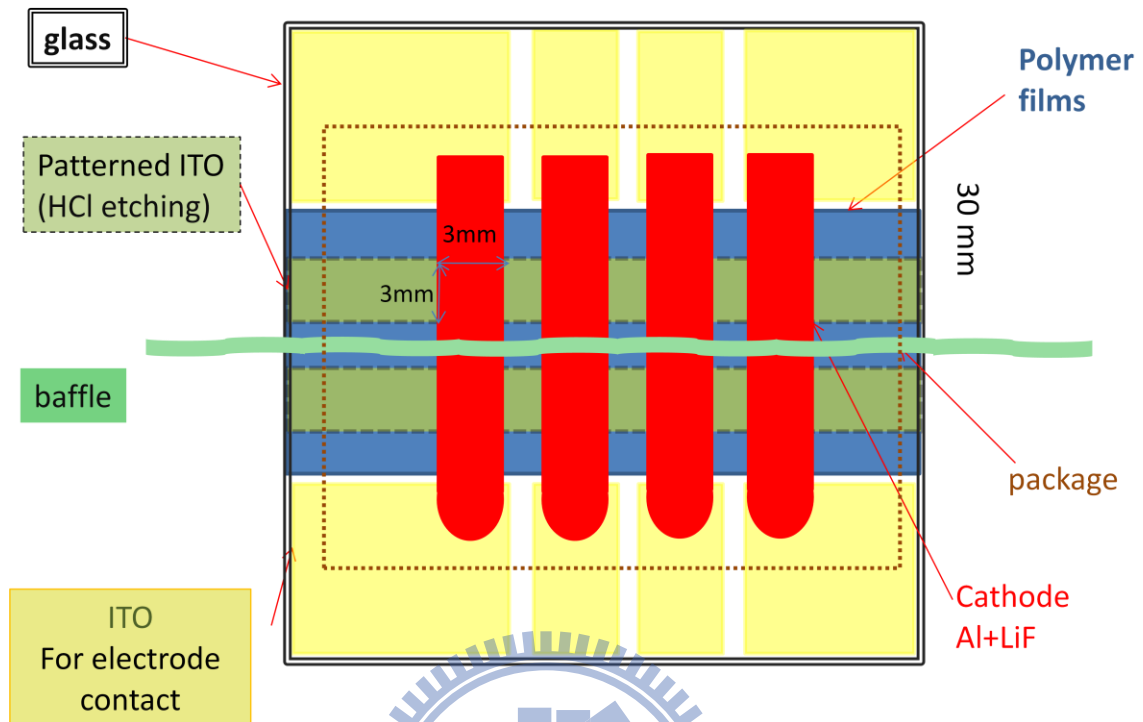
Figure 3-9 The perspective drawing of the finished device.

3.3 Measurements

PL and optical absorption were carried out by Acton Research Spectra Pro-150 and PerkinElmer Lambda 650, respectively. The thickness of film was measured by alpha-step and AFM. The voltage-current-luminance characteristics were measured using an optical power meter (PR-650) and digital source meter (Keithley 2400). In our research, Ultraviolet-Visible spectroscopy and photoluminescence spectroscopy offer rigorus measurements of plasmon resonance band of Au NPs and the system between light-irradiated particle and active layer, respectively. In the following section **(3-9)**, **(3-10)**, a detail introduction of them will be given.

3.3.1 Ultraviolet-Visible (UV-Vis) Spectroscopy

A scheme of the components of a simplified spectrometer **(Figure 3-10)** is shown in the following diagram. An incident light (colored red) comes from two sources, visible or UV
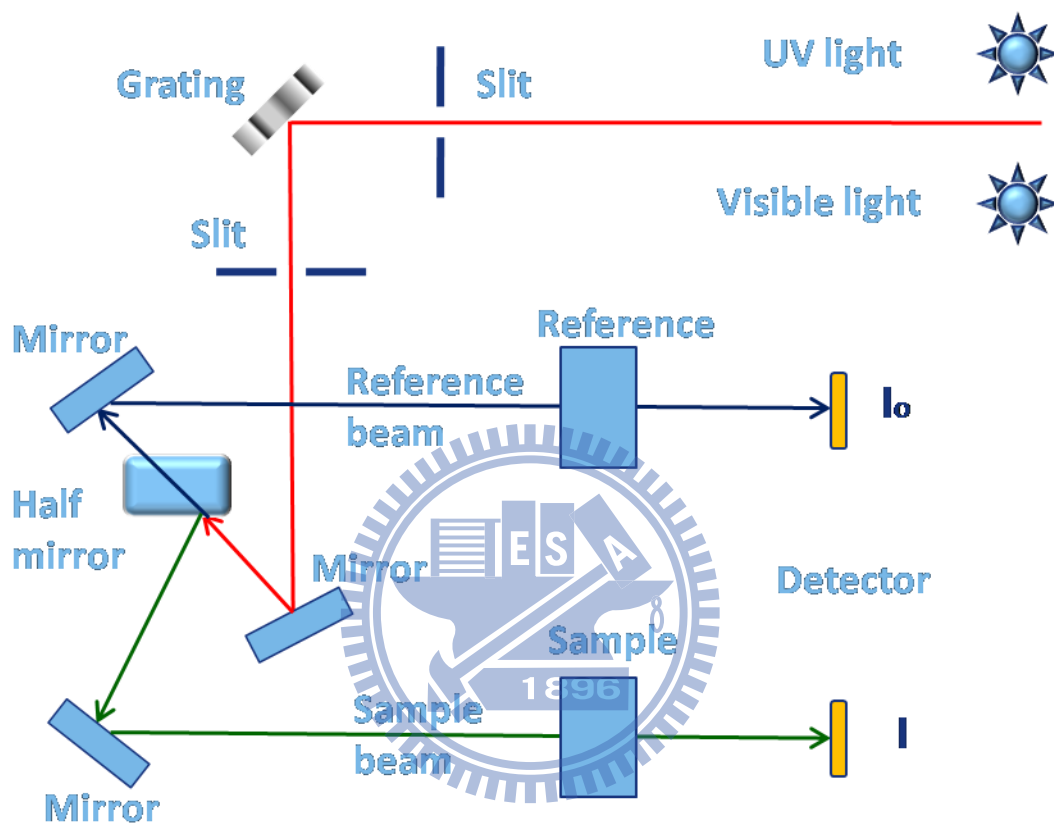
Figure 3-10 Scheme of the components of UV-Vis Spectroscopy

light. Each single wavelength is extracted by a prism or diffraction grating, and the beam of light is split into two equal intensity beams by a half-mirrored component. The sample beam (Green magenta) passes through the examined sample. The reference beam (colored blue) passes through an identical substrate of sample. The substrate depends on what the materials you want to make it as a reference. For gold colloid, it is cuvette containing only the D.I. water, and for quartz-substrate samples, it is only the quartz substrate. The intensities of these light beams are then measured by electronic detectors and compared. The intensity of the reference beam, which should have suffered little or no light absorption, is defined as I_0. The

intensity of the sample beam is defined as **I**. Over a short period of time, the spectrometer automatically scans all the component wavelengths in the manner described. The ultraviolet (UV) region scanned is from 200 to 400 nm, and the visible portion is from 400 to 800 nm. Absorption is defined as $A= \log \mathbf{I_0/I}$. If no absorption has occurred, $A= 0$. The wavelength of maximum absorbance is a characteristic value, designated as λ_{max}. Different examined samples may have very different absorption maxima and distribution of absorption. For absorbing intensely sample, it must be examined in dilute solution, so that the passed light received by the detector is significant, and to use transparent solvents to prevent extra absorption.
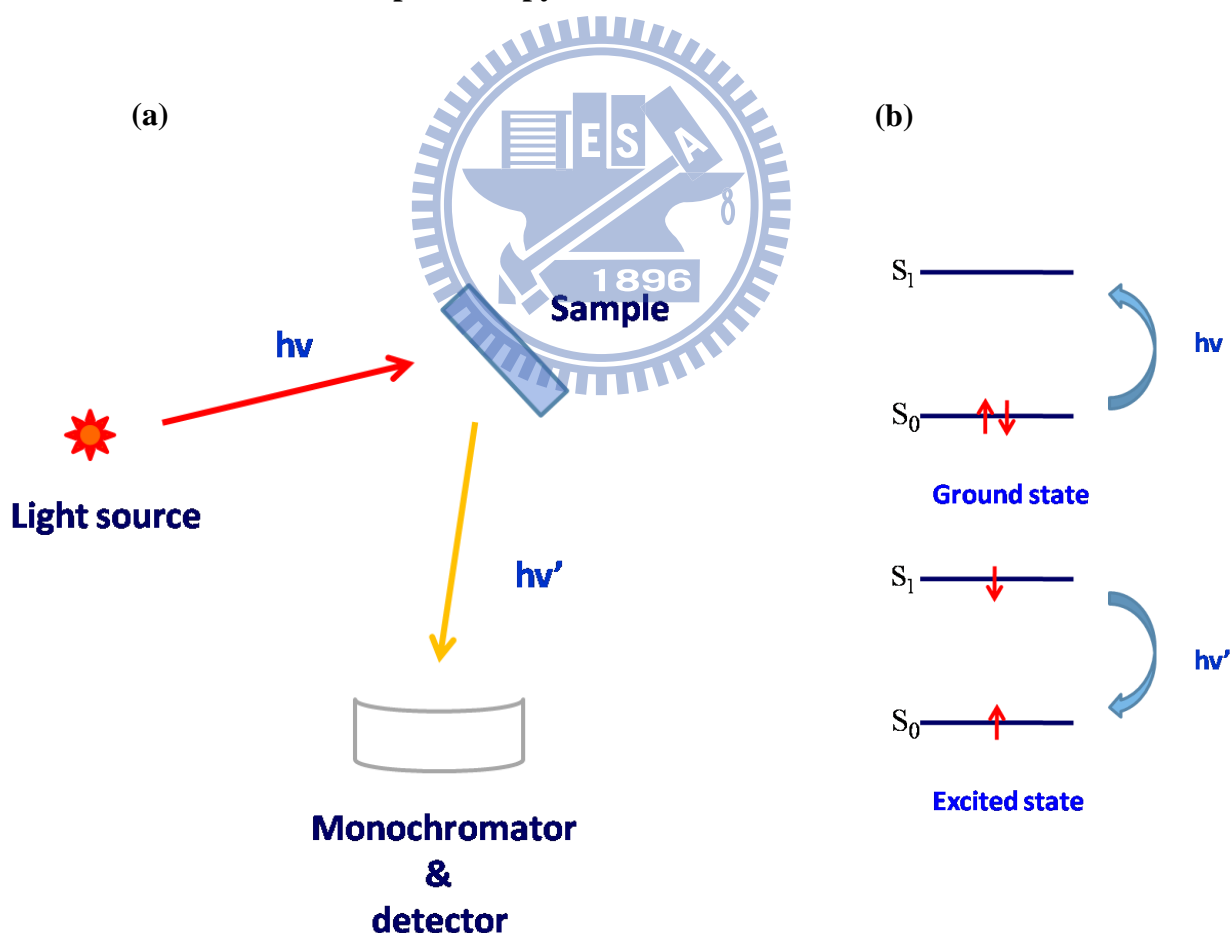
3.3.2 Photoluminescence Spectroscopy

Figure 3-11 (a) A simple scheme of the Photoluminescene Spectroscopy
(b) An energy-transfer diagram of photoluminescence

A scheme of the photoluminescence apparatus is shown in **Figure 3-11(a)**. Photoluminescence is excited by an unpolarized light (wavelength of the light is adjustable). The luminescence radiation is filtered by a monochromator and detected by a detector. The PL signal is amplified by a Photomultiplier tube (PMT). And the detector is on the same side of the incident light with the same incident angle to the normal of the sample. Photoluminescence (abbreviated as PL) is a process in which a substance absorbs photons (electromagnetic radiation) and then re-radiates photons **(Figure 3-11(b))**. Quantum mechanically, this can be described as an excitation to a higher energy state and then a return to a lower energy state accompanied by the emission of a photon. This is one of many forms of luminescence (light emission) and is distinguished by photoexcitation (excitation by photons). The period between absorption and emission is typically extremely short, in the order of 10 nanoseconds. Under special circumstances, however, this period can be extended into minutes or hours. More interesting processes occur when the chemical substrate undergoes internal energy transitions before re-emitting the energy from the absorption event. The most familiar such effect is fluorescence, which is also typically a fast process, but in which some of the original energy is dissipated so that the emitted light photons are of lower energy than those absorbed. The generated photon in this case is said to be red shifted.

Chapter 4

Results and Disscussions

4.1 Surface Plasmon Characterization of Gold Nanoparticles

When gold nanoparticles interact with an electromagnetic wave, a unique resonance behavior occurs at visible spectrum. The phenomenon leads to localized surface plasmon which depicts the non-propagating excitations of conduction electrons of metallic nano-structures coupled to photons. At the beginning, we explored the physical insight into the optical characteristics of gold nanoparticles.
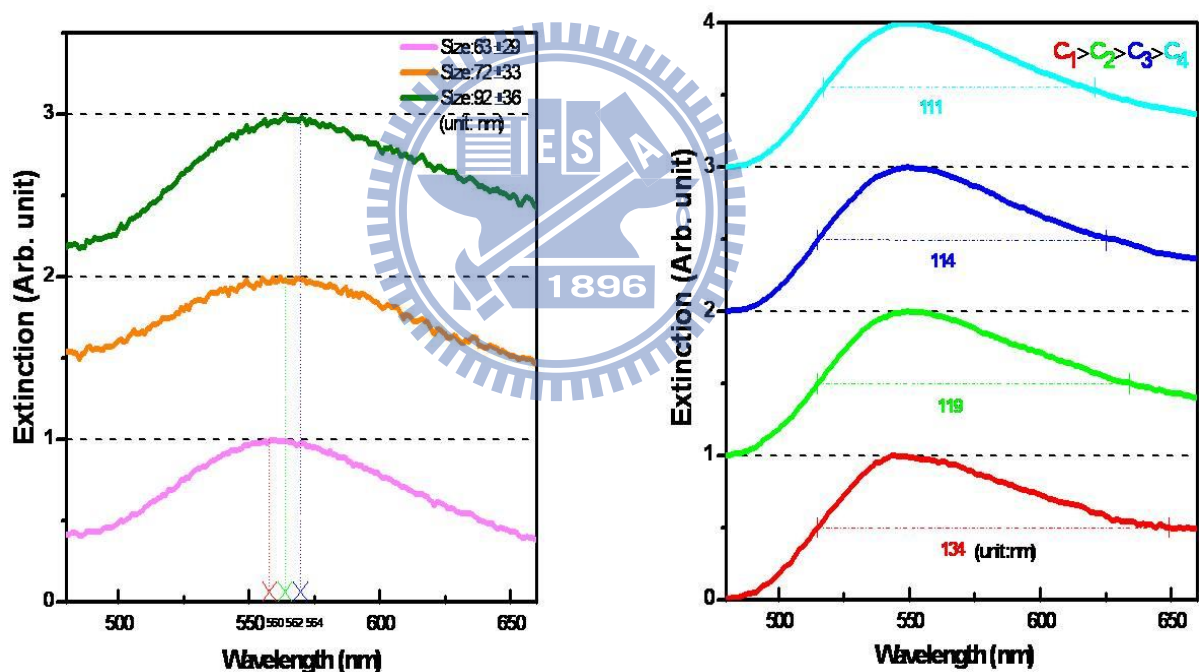

Figure 4-1 Surface plasmon extinction spectra of spherical Au nanoparticles, with **(a)** different Au nanoparticles sizes and **(b)** different Au nanoparticles concentration (C1, C2, C3,and C4)

Extinction spectra for average Au nanoparticles size 63, 72, and 92 nm in diameter suspended in aqueous solution are shown in **Figure 4-1(a)**. The extinction spectra of gold NPs

exhibit a dependence of particle sizes due to resonantly enhanced absorption and scattering. From **Figure 4-1**, it can be observed that the surface plasmon absorption resulted in red shift with increasing the particle size.

For nanoparticles radius r much small smaller than the wavelength of the incident light (roughly $2r < \frac{\lambda_{max}}{10}$), dipole oscillation significantly contributes to the extinction cross-section and explained by dipole approximation of the Mie theory [20]. However, for larger nanoparticles where the dipole approximation is no longer valid, the plasmon resonance depends explicitly on the particle as a function of particle radius. The larger the particle become, the more important are the higer-order modes. At this time, the light can no longer polarize the nanoparticles homogenously. The higher-order modes peak at lower energies and therefore the plasmon band redshifts with increasing particle size.

on the other hand, the concentration increase results in a widening bandwidth, while the plasmon bandwidth is associated with the dephasing of the coherent electron oscillation **Figure 4-1(b)**. Large bandwidth corresponds to increasing loss of the coherent electron motion. In the following section, NPs with the most dilute concentration (C_4= 0.1 w.t.%) and with the largest radius (r=92±36 nm) were adopted since their absorption peak overlaps that of the fluorescence emitter.

4.2 Fluorencense Enhancement by nanocomposite

In this section, we blend gold nanoparticles into PEDOT:PSS to form a nanocomposite material which is capable to manipulate the photon coupling from emitting photons with the non-propagating surface plasmon. Au-incorporated nanocomposite offers the ability to study local electromagnetic interactions in the plasmon-fluorenscense system. The example of fluorescent emitter, MEH-PPV, located in proximity to the surface plasmon polariton field of the metal is a case in point here.
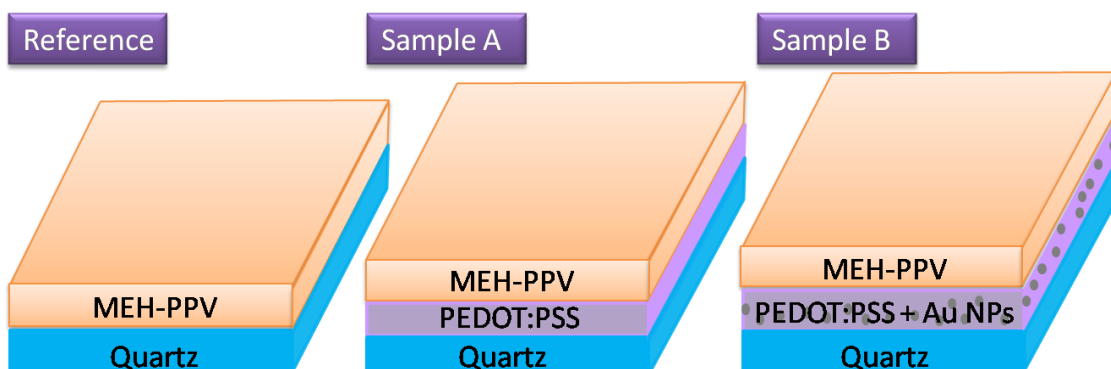
Figure 4-2 Cross-section of the samples (R, A, and B)

Three samples were prepared as shown in **Figure 4-2**. Sample R is a bare MEH-PPV layer spin-coated on the quartz substrate as a reference, sample A is the PEDOT:PSS layer inserted into the structure of sample R, and sample B replaces the PEDOT:PSS layer with Au
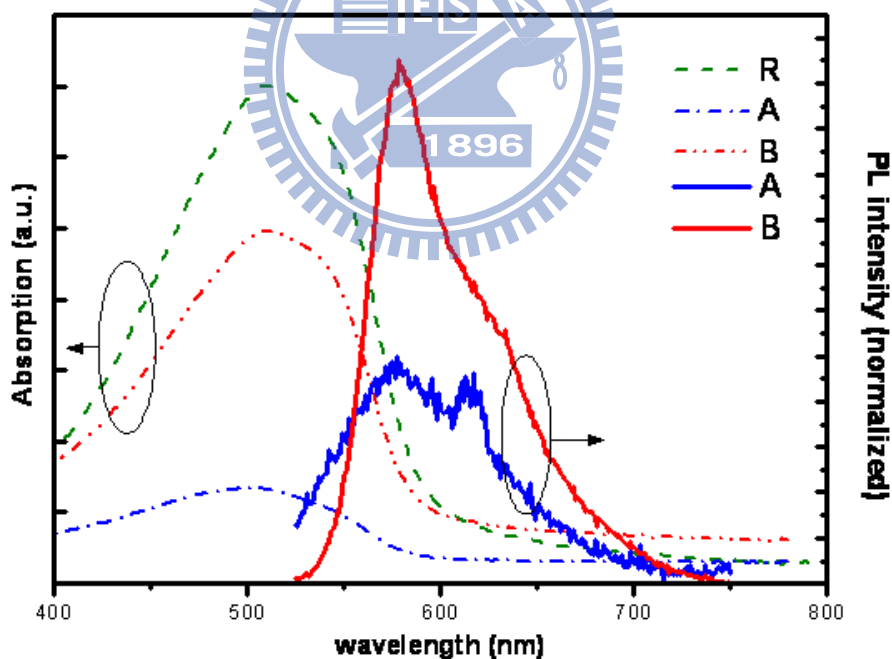

Figure 4-3 Absorption and photoluminescence spectra of samples with (sample B) and without (sample A) gold-incorporated nanocomposite layer.

nanoparticles-incorporated PEDOT:PSS nanocompsite layer. The sample design includes practical features which aim at the utilization of the exciton-plasmon interaction in an optoelectronic device.

The observed PL as well as absorption spectra is plotted in **Figure 4-3**. While fluorescence emitted from MEH-PPV passed through the PEDOT:PSS layer as a reference, the FWHM of the PL spectrum is about one-half of the absorption spectrum and has a vibronic feature in the shoulder at the long-wavelength region [24]. The respective emission peaks (normalized) represent vibrational transitions between energy levels：0-0 and 0-1. However, as the fluorescence coupled with nanocomposites, the presence of noble metal surfaces can significantly impact the manner in which incident photoexcitation was converted into photons. The relative contribution of absorption and radiative scattering to the overall extinction spectrum of a metal nanostructure is a crucial factor that dictates the conversion efficiency of incident photons to fluorescence emission from the nanoparticles/emitter system.

This interesting phenomenon can be explained by the radiating plasmon (RP) model [1], where plasmons induced by resonant near-field interactions of fluorescence emitter with

Material	(nm)	Peak (nm)	Stokes Shift (nm)	1931 CIE x,y	PL FWHM (nm)	R. Q. E. R.[a] (a.u.)
Sample R	513	596	83	(0.60,0.40)	61	—
Sample A	500	577	77	(0.51,0.49)	119	1.00
Sample B	511	578	67	(0.55,0.45)	72	2.30

Table 4-1 Optical properties of test samples and their corresponding photoluminescence (PL) characteristics. R.Q.E.R. is defined as a relative quantum efficiency ratio, which denotes the quantum efficiency in contrast to the no nanoparticles incorporated sample (sample A).

metallic nanostructures (having dominant scattering properties) will radiate the spectral properties of the excited state intensely, thereby leading to observations of emission enhancements even from the fluorescence emitter with high free space quantum yields. The lower shoulder peak accounting for the 0-1 state energy transition (at 614 nm) is relatively suppressed for no surface plasmon mediated interplay with the nanoparticles, and FWHM of overall emission spectrum was thus minimized. According to **Table 4-1**, the emission of sample B peaked at 577 nm with a narrow FWHM, that incurs a red saturated color corresponding to 1931 Commission Internationale de l'Éclairage (CIE) color coordinates of (0.55, 0.45). To sum up, the narrowed FWHM of bandwidth implied the rising amount of radiative emission into visible region and the furthering of the radiative efficiency, which is a promising characteristic for electroluminescence of potential applications as PLEDs.

To make a brief summary, gold NPs-incorporated PEDOT:PSS was demonstrated in nanocomposite forms. We have also investigated the optical properties of insertion of nanocomposite layer which led to surface plasmon mediated photoluminescence enhancement from the emissive layer, MEH-PPV. Surface plasmon polariton resonance coupling to molecular excited state resulted in enhancement of up to 2-fold in overall relative quantum efficiency. Meanwhile, the photoluminescence spectra peaked a more saturated color corresponding to 1931 CIE coordinates of (0.55, 0.45) stemmed from the more narrow bandwidth feature. These samples designed with practical features target at the eventually performance optimization of the polymeric optoelectronic device by exciton-plasmon interaction.

4.3 Optimal Fluorencense Enhancement by nanocomposite

We have known the optical properties of dispersion of Au nanoparticles into polymer matrix which led to surface plasmon mediated photoluminescence enhancement from the emissive layer, MEH-PPV. Surface plasmon polariton resonance coupling to molecular excited state resulted in enhancement of up to 2-fold in overall relative quantum efficiency. It is known that luminescence can be enhanced near the metallic nanostructures, however in this section we wonder to know whether the optimal fluorescence enhancement can be achieved at a resonant distance between nanocomposite and emission layer.

In order to build a tunable distance between the Au particles and emissive polymer, we insert a PEDOT:PSS layer to form a spacer layer which the thickness (d) can be controlled by adjustable r.p.m. (revolution per minute) of the spinner. **Figure 4-4** shows the structure with introducing the spacer layer. The different thickness of spacer layer with 0 nm, 10 nm, 30 nm, 40 nm, 60 nm,

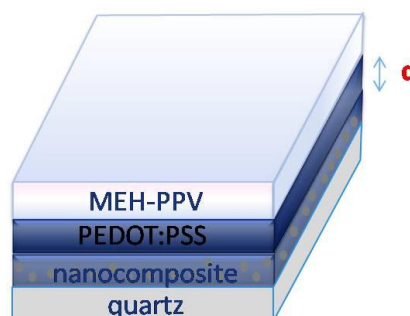**Figure 4-4** The inserted PEDOT:PSS layer between emission layer and nanocomposite plays an role of spacer layer, and a resonant distance may help to obtain an optimal fluorescence enhancement.
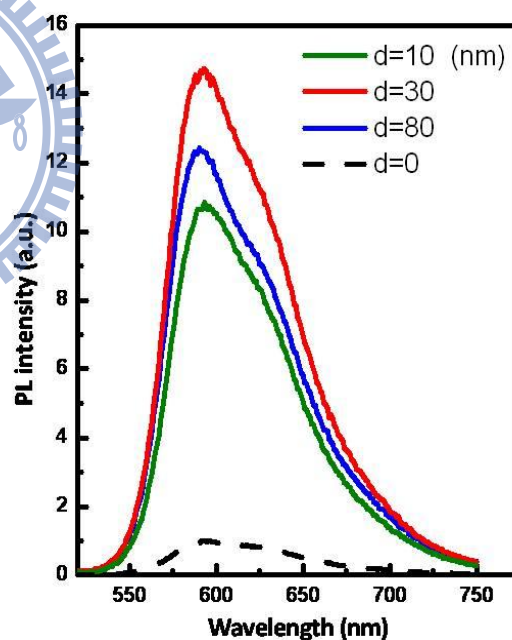

Figure 4-5 By tunable thickness of spacer layer with 0nm, 10nm, 30nm, 80nm, the different order of PL intensity can be enhanced. The PL intensity is normalized at the sample without spacer layer (d=0 nm).

and 80 nm, were respectively deposited into the location between emission layer and nanocomposite. The observed PL intensity is shown in **Figure 4-5**. (The 40 nm and 60 nm curves almost overlap with the other curves so that for clearing figure showing, we don't put them on this figure.) The PL intensity of each thickness is normalized by the curve without spacer layer (d=0 nm). **Figure 4-5** shows a result that the PL intensity get enhancement by adding the spacer layer, especially with the thickness of 30 nm. The result revels that luminescence can be enhanced near the metallic nanostructures, and tuning the distances between nanocomposite and emission layer can even directly increase the radiative intensity of emissive polymer.

At a resonant distance, the optimal fluorescence enhancement can even be obtained. Dipolar mode of localized surface plasmon at gold NPs with average sizes 92 nm is more remarkably coupled with singlet polaron excitons in MEH-PPV layer, which in nature perform dipolar behavior. Furthermore, inserting a spacer layer tunes the distances of resonant coupling between dipoles and excitons. For a configuration

Figure 4-6 Color modulation of different structure of samples on CIE 1931 color space

with a spacer layer of width *d* as 30 nm, the PL enhancement can be as high as 15x than the sample without spacer layer (d=0 nm). An additional result reveals that the color coordinates of different structure of each sample can be altered. It offers a color modulation way by altering layer structure (**Figure 4-6**).
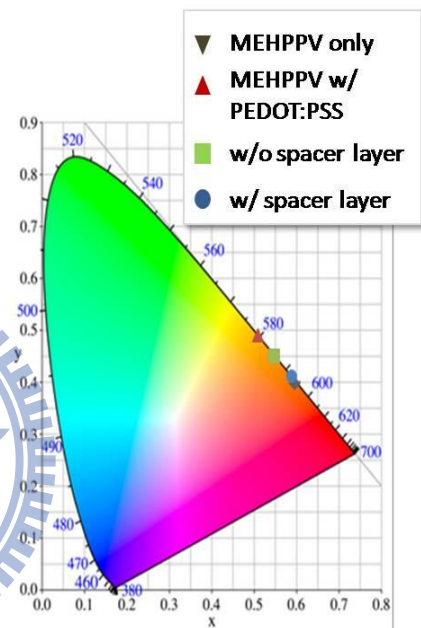
4.4 R. Q. Y. R. (relative quantum yield ratio) V.S. Distance

R. Q. E. R. is defined as relative quantum efficiency ratio, which denotes the quantum efficiency in contrast to the no NPs-incorporated sample (sample A). The R. Q. E. R. versus to variable thickness of spacer layer is shown in **Figure 4-7**. The black line corresponds to dipole approximation of theoretical analysis (**Figure 2-6**). The R. Q. Y. R. of each various thickness from experimental results is fitted by red curve. At the region of distance $d > 30nm$ (red area), the nanoantenna approximation has been proven validly. It reveals that the enhancement of luminescence versus different d was decided by near-field effect at longer distance d. However,

Figure 4-7 R.Q.Y.R. as a function of d between the emitting layer and the nanoantennas. Black line shows the theoretical results by the exact electrodynamical method at the dipole approximation.

the black line (**Figure 4-7**) corresponds to the dipole approximation which fails for short distance d ($d < 30nm$). On the other hand, for the distance d is smaller than 30 nm, the emitters reach a strong coupling regime with the nearby nanoparticles. Not only the quenching but also the enhancement of quantum yield will be amplified and respectively attributed to the increasing non-radiative decay rate and radiative decay rate with decreasing distance. Since electric field in the sphere is a superposition of all multipole modes, all these
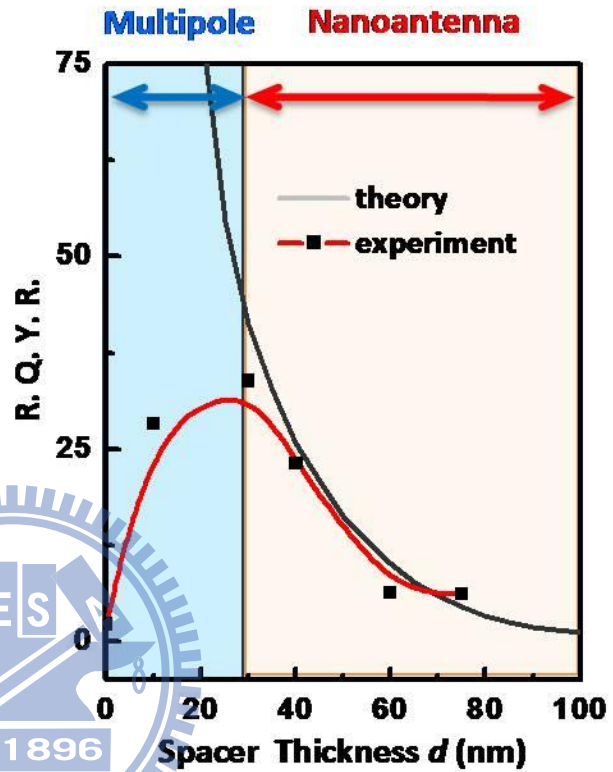
modes contribute to the non radiative decay rate, whereas only the dipole mode is assumed to affect the radiative decay rate. The dipole approximation strongly overestimates the quantum yield at short distance and does not predict any quenching. Furthermore, the conformational defects also introduced a potential quenching channel such as trapping states at the interfaces.

4.5 Characteristic of Electroluminesecence on the Device
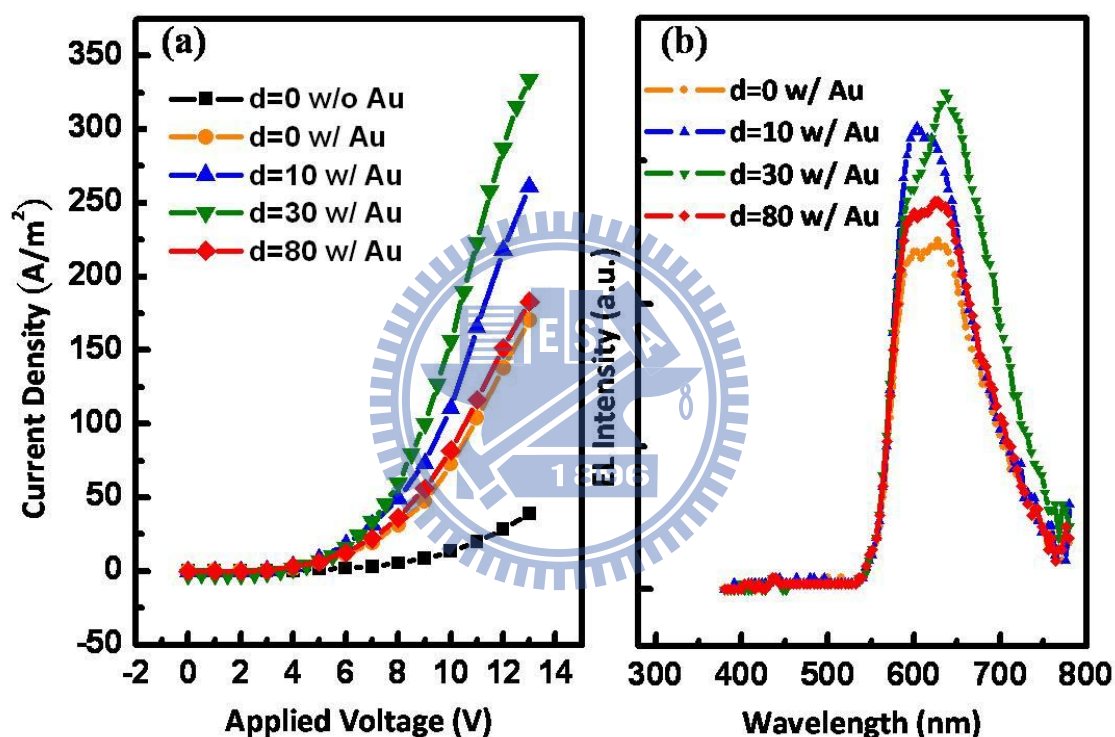
Figure 4-8 (a) current density-voltage and **(b)** EL spectra characteristics of polymer light emitting devices made with the PEDOT:PSS and the PEDOT:PSS-Au nanocomposites with different thickness of spacer layer.

Current density (J)-Voltage (V), and EL spectra characteristics of various devices fabricated in this work are shown in **Figure 4-8**. It is noteworthy that the performance of the PLEDs is significantly improved when the PEDOT:PSS-Au nanocomposite layer is used compared to the one using PEDOT:PSS only as a hole injection layer. Especially for

using PEDOT:PSS-Au nanocomposite layer with a spacer layer of thickness d=30 nm, the electronic characteristic is improved strongly. At electroluminescence, highest EL intensity of proposed scheme were observed at d=30 nm as predicted by PL measurement and optical model. The results reveal that introduction of nanocomposite layer and spacer layer did not deteriorate electrical performance in PLED, whereas the luminescent quantum efficiency can be enhanced.
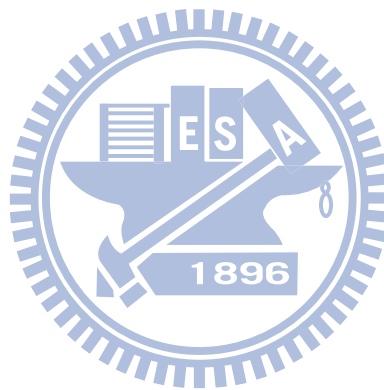
Chapter 5

Conclusion and Future Work

5.1 Conclusion

Surface plasmon resonances in metallic nanoparticles are of interest for a variety of applications due to large local field enhancement that occurs in the vicinity of metal surface. And a metallic nanoparticle sphere acts as a nanoantenna in the quasi-static dipole approximation limit of Mie theory. In this study, gold NPs-incorporated PEDOT:PSS was demonstrated in the nanocomposite form. The dipole mode of localized surface plasmon at gold NPs with diameter as average size 92 nm remarkably coupled with singlet excitons in the MEH-PPV layer, which in nature perform dipolar behavior. Theory predicted that spectral behaviors of coupled excitation in excitons are modulated by the separation due in part to the near-field effect of localized surface plasmon and in part to the Purcell effect, while the nanoantenna assumption only applied at long distances. These predictions were confirmed in

sample	reference		nanocomposite structure	
	MEHPPV only	MEHPPV with PEDOT:PSS	without spacer layer ($d=0$)	with spacer layer ($d=30$)
Max Absorption Peak (nm)	513	500	511	502
Max Photoluminescence Peak (nm)	596	577	578	593
FWHM(nm)	61	119	72	77
Stokes Shift (nm)	83	77	67	90
1931 CIE x,y	(0.60,0.40)	(0.51,0.49)	(0.55,0.45)	(0.59,0.41)
Relative Quantum Yield Ratio (R.Q.Y.R.)	—	1.00	2.30	>30

Table 5-1 Comparisons of the characteristics of various configurations

a nanostructured polymeric system by inserting a bare PEDOT:PSS layer as spacer to tune the spatial overlap between dipoles and excitons. Combination of nanocomposite and spacer layer discloses the merit of metal enhanced fluorescence (MEF) effect, as well as color tunability.

Compared to the sample without Au particles mixing into PEDOT:PSS layer, surface plasmon resonance coupling to molecular excited state resulted in fluorescence enhancement of up to 2.3-fold in overall relative quantum efficiency. Optimal design of spacer layer (30 nm) enhances the Q.Y. as high as 30x. By inserting of nanocomposite and spacer layer, not only the optical efficiency can be effectively enhanced without sacrifice the electric properties. Dual-functional nanocomposite plays the role of hole-injection layer in organic lighting devices, and possesses potential for photovoltaic applications.

5.1 Future work

Although the structure with optimal Q.Y. has been realized in photoluminescent results, some issues regarding electroluminescence have to be expounded. Firstly, the roughness of nanocomposite layer and interface morphology can pronouncedly affect the charged carrier injection. EL quantum efficiency η_ϕ related to PL intrinsic quantum efficiency η_{em} by

$$\eta_\phi = \gamma \times \eta_r \times \eta_{em}$$

where γ is a balanced charge injection factor, which is depend on the processes of carrier injection, and η_r quantifies the efficiency of the formation of a singlet exciton from a positive and a negative polaron. We expect the width of spacer layer d and the existence of nanoparticles are relevant to γ. However, the mechanism depicting the interplay between injected charged carriers and nanoparticles is still ambiguous. We hope EL measurement will help us unveil the underlying relationship between η_ϕ and η_{em}.

Reference

[1]   J. R. Lakowicz, *Plasmonics* **1**, 5-33 (2006)

[2]   E. Fort, S. Gresillon, *J. Phys.* D 41, 013001 (2008)

[3]   P. P. Pompa, L. Martiradonna, A. D. Torre, F. D. Sala, L. Manna, M. de Vittorio, F. Calabi, R. cingolani and R. Rinaldi, *Nature Nanotechnology* **1**, 126 (2006)

[4]   K. Aslan, I. Gryczynski, J. Malicka, E. Matveeva, J. R. Lakowicz, C. D. Geddes, *Current opinion in biotechnology*, **16**, 55 (2005)

[5]   http://www.britishmuseum.org/explore/highlights/highlight_objects/pe_mla/t/ the_lycurgus_cup.aspx

[6]   M. Faraday, *Philos. Trans. Royal Soc.* London, **147**, 145 (1857)

[7]   G. Mie, Ann, *Phys.*, **25**, 377 (1908)

[8]   U. Krebig, M. Vollmer, Optical Properties of Metal Cluster, Springer Verlag, Berlin (1996)

[9]   L.M. Liz-Marzán, *Mater. Today* **7**, 26, (2004)

[10]   T. D. Neal , K. Okamoto, and A. Scherer, *Opt. Express* **13**, 5522 (2005)

[11]   E. M. Purcell, *Phys. Rev.*, **69**, 681 (1946)

[12]   I. M. Soganci, S. Nizamoglu, E. Mutlugun, O. Akin, H. V. Demir, *Opt. Exp.* **15**, 14289(2007)

[13]   J.-H. Song, T. Atay, S. Shi, H. Urabe, A. V. Nurmikko, *Nano Lett.* **5**, 1557 (2005)

[14]   V. Thomas, M. Namdeo, Y. M. Mohan, S. K. Bajpai, M. bajpai, J. *Macromolecular Science* A 45, 107 (2007)

[15]   B. K. Kuila, A. Garai, and A. K. Nandi, *Chem. Mater.* **19**, 5443 (2007)

[16]   B. Y. Kim, M. S. Cho, Y. S. Kim, Y. Son, Y. Lee, *Synthetic Metals* **153**, 149 (2005)

[17]   J. Mathiyarasu, S. Senthilkumar, K. L. N. Phani, V. Yegnaraman, *Mater. Lett.* **62**, 571

(2007)

[18]　J. Liu, K. Kim, D. L. Carroll, *Synthetic Metals* **157**, 580 (2007)

[19]　J.- W. Park, Md. H. Ullah, S. S. Park, and C.- S. Ha, *J., Mater. Sci.* **18**, S393 (2007)

[20]　C. F. Bohern, D. R. Huffman, Absorption and Scattering of Light by Small Particles, Vol. 1, John Wiley and Sons, Inc., New York (1998)

[21]　P. Anger, P. Bharadwaj, L. Novotny, *Phys. Rev. Lett.* **96**, 113002 (2006)

[22]　S. Kuhn, U. Hakanson, L. Rogobete, V. Sandoghdar, *Phys. Rev. Lett*. **97**, 017402 (2006)

[23]　B. Park, S. Jeong, D. Kim, J. Moon, S. Lim, J. Kim, *J. Colloid and Interface Sci.* **311**, 417 (2007)

[24]　R. Chang, J. H. Hsu, W. S. Fann, K. K. Liang, C. H. Chang, M. Hayashi, J. Yu, S. H. Lin, E. C. Chang, K. R. Chuang, S. A. Chen, *Chem. Phys. Lett.* **317**, 142 (2000)